Evaluation of Systematic Errors on Polarization Parameters from POLDER Instrument Data for Use In CLARREO Pathfinder-VIIRS Intercalibration

Daniel Goldin[a,b,*], **Rajendra Bhatt**[b], **Yolanda Shea**[b]
[a]ADNET Systems, Inc., Bethesda, MD 20817, USA
[b]NASA Langley Research Center, Hampton, VA 23666, USA

Abstract. One of the CLARREO Pathfinder (CPF) mission's science objectives is to intercalibrate the reflective solar bands of the NOAA-20 VIIRS instrument against high-accuracy CPF measurements utilizing coincident, co-angled, and co-located footprints acquired over diverse Earth targets. To alleviate the effect of high polarization sensitivity of select VIIRS channels on intercalibration analysis, the CPF team will limit the intercalibration footprints over low-polarized scene types, which will be identified based on an empirical estimation of their degree and angle of polarization (DOP and AOP) using POLDER data. This paper describes the methodology for evaluating systematic errors in the estimation of DOP and AOP for Earth-reflected radiances using POLDER's polarized bands and investigates their potential impact on CPF-VIIRS intercalibration uncertainty. The systematic errors were found to be less than 0.01 for DOP and less than 2.2° for AOP, which will have a negligible impact on CPF-VIIRS intercalibration uncertainty.

Keywords: polarization, systematic, uncertainty, CPF, CLARREO, VIIRS.

*Daniel Goldin, daniel.goldin@nasa.gov

1 Introduction

NASA's Climate Absolute Radiance and Refractivity Observatory (CLARREO) Pathfinder (CPF)[1] is an Earth-viewing reflected solar spectrometer that will measure the Earth-reflected solar radiation from the International Space Station with a radiometric uncertainty of 0.6% (1σ) traceable to the standards of the International System of Units, known as "SI-traceability". The high-accuracy measurements will provide a reference for intercalibrating other in-orbit reflective solar instruments. The spectral range of the CPF instrument is 350-2300 nm, with resolution of 6 nm and 3 nm sampling rate. The CPF's state-of-the-art intercalibration approach will demonstrate the ability to accurately transfer the CPF reference calibration to the shortwave channel (300-5000 nm) of the Clouds and the Earth's Radiant Energy System (CERES) instrument[2] and the reflective solar bands (RSBs) of the Visible Infrared Imaging Radiometer Suite (VIIRS) instrument,[3] both onboard the NOAA-20 spacecraft. The aimed-for intercalibration uncertainty for both target instruments is also 0.6% (1σ). To satisfy this stringent constraint the CPF team has developed methods for mitigating the impacts of spatial, spectral, polarization, and angular differences between the intercalibration footprints from the CPF and target instruments.

The polarization sensitivity of an instrument may be characterized by evaluating its diattenuation coefficient. The CPF instrument is designed to have low polarization sensitivity, with the diattenuation coefficients less than 0.01 for wavelengths below 1800 nm and less than 0.02 above 1800 nm. Of the two intercalibration target instruments, the VIIRS sensor has a significantly higher polarization sensitivity, with diattenuation coefficients up to 0.06 for select shortwave RSBs,[4,5] which has the effect of biasing the intercalibration over highly polarized Earth scenes. To mitigate this impact, the CPF team has developed Polarization Distribution Models (PDMs) to characterize the polarization state in terms of degree of polarization (DOP) and angle of polarization (AOP) of the

Earth-reflected radiance as a function of the intercalibration footprint scene type, solar and viewing geometry, and wavelength[6,7]. The PDMs will assist in identifying low-polarized scene radiances by meticulously intercalibrating the polarization-sensitive VIIRS RSBs against the CPF measurements. The empirical PDMs (ePDMs) are derived using the multidirectional Earth-reflected polarized solar radiation measurements from visible and near-infrared channels of the POLarisation and Directionality of the Earth's Reflectances (POLDER) instrument[8,9] mounted onboard the Polarisation and Anisotropy of Reflectances for Atmospheric Science coupled with Observations from a Lidar (PARASOL) micro-satellite that was operational between 2004 and 2013. The theoretical formulation of the polarization parameters for Earth-reflected radiances using Stokes parameters and their impacts on the at-sensor measurements is discussed below.

A polarization state at the top of the atmosphere (TOA) is specified by three Stokes parameters I, Q, U where I is radiance, and Q and U describe linear polarization. (In the context of most of the TOA remote sensing applications, the fourth Stokes parameter, V, is negligibly small and can be ignored.) Alternatively, a polarization state may also be described by the degree and angle of polarization, DOP and AOP, expressed in terms of the Stokes components. Throughout the text we assume Stokes parameters Q, U and I to be normalized to the ratio of spectral radiance I over irradiance at nadir, multiplied by π and are, therefore, taken to be unitless. The degree of polarization, DOP, which we will alternately denote as P, may be expressed in terms of the ratio of the Stokes parameters as:

$$P = \frac{\sqrt{Q^2 + U^2}}{I} \tag{1}$$

From this definition it follows that the polarization state can range from completely unpolarized ($Q = 0, U = 0$) to fully polarized ($I = \sqrt{Q^2 + U^2}$).

We denote the angle of linear polarization relative to the scattering plane as ψ. The light scattered in the atmosphere is predominantly s-polarized, so that ψ values are found mainly around $90°$. The angle of linear polarization may also be defined relative to the meridian, or detector, plane and can be expressed in terms of the Stokes parameters as:

$$\chi = \frac{1}{2}\arctan(U/Q). \tag{2}$$

The two polarization angles, χ and ψ are related as

$$\psi = \chi - \alpha, \tag{3}$$

where α may be expressed in terms of the three view geometry variables, relative azimuth (RAZ), solar-zenith and view-zenith angles (SZA and VZA, respectively), as[10]

$$\tan\alpha = \frac{\sin(\mathrm{SZA})}{\frac{\sin(\mathrm{VZA})}{\tan(\mathrm{SZA})} - \cos(\mathrm{VZA})\cos(\mathrm{RAZ})}. \tag{4}$$

By default it is the angle χ that is being referred to as the angle of polarization (AOP) throughout the text. In the forward scattering region, the clear-sky scene types are well-approximated by single scattering with the scattering angle defined here as (see, e.g., Ref. 11)

$$\cos\Theta = -\cos(\mathrm{VZA})\cos(\mathrm{SZA}) - \sin(\mathrm{VZA})\sin(\mathrm{SZA})\cos(\mathrm{RAZ}). \tag{5}$$

When the light incident upon a detector is polarized and the detector itself is polarization-sensitive the relationship between the uncorrected and corrected reflectances is given by:[5,12]

$$\rho \equiv c_\rho \rho_0 = \frac{\rho_0}{1 + aP\cos 2(\chi + \phi)} \tag{6}$$

where ρ_0 is the uncorrected reflectance and ρ is the reflectance corrected for detector polarization effects, a is the detector diattenuation coefficient and ϕ is the phase shift caused by the detector.The Stokes parameters provided by the POLDER's polarized bands, centered at 490, 670 and 865 nm, are used to construct the ePDMs that quantify the effects of polarization due to scattering in the atmosphere and off Earth's surface. These ePDMs provide DOP and AOP values for CPF-VIIRS intercalibration samples and are categorized based on surface type, atmospheric conditions, solar and view geometry.[12] Each ePDM is binned in relative azimuth (RAZ) and view zenith angle (VZA) and is constrained to a specific solar zenith angle (SZA) range. For every ePDM bin a mean DOP (or AOP) value is computed from the Stokes parameters. In addition to the means, the corresponding standard deviations are recorded in the same view and solar geometry format as the means. In an idealized ePDM these standard deviations would be dominated by random uncertainties, also, ideally, small. This would enable us to improve the intercalibration accuracy by increasing the data sample, as accuracy scales with the square root of the sample size. However, since the ePDMs rely on detector measurements they are also susceptible to systematic errors. These errors are characterized by a probability distribution whose mean we will refer to as "bias" and its width as the "systematic uncertainty." We will use the term "systematic error" as encompassing both bias and the systematic uncertainty. While measurement bias can often be corrected, systematic uncertainty is irreducible.

Among the many sources of noise in a charge coupled detector, such as POLDER, there are two dominant sources (see, e.g., Ref. 13, 14): external photon noise and detector noise. The photon noise is due to fluctuations in the number of photons entering the detector which may be described by the Poisson distribution (or Gaussian distribution for a large enough statistical sample) whose variance is proportional to radiance. Two sources dominate the detector noise: the dark-current noise in electronics and readout (read) noise, which depends on the frame rate and sampling frequency. In practice, using the data from in-orbit instrument it is difficult to isolate random photon noise from from Rayleigh or Mie scattering in the atmosphere, much less to attribute the type of noise to its source, so from here onward we will use the term "noise" loosely, insofar the empirical observations allow.

Due to the non-negligible polarization sensitivity in some of the VIIRS shortwave channels, as described above, during the initial year of CPF-VIIRS intercalibration the DOP selection will be constrained to be less than 0.1. As we will demonstrate later in this article, the effect of noise is to bias DOP means towards higher values, with the implication that the $\mathrm{DOP} < 0.1$ intercalibration sample might be selecting DOP values higher than "true" mean DOP. As CPF strives to achieve the lowest possible intercalibration uncertainty, the focus of this work is to quantify this bias. In addition, a bias in DOP, as well as any potential bias in AOP, will affect the precision of determination of the reflectance (see Eq. 6).

The effects of noise manifest themselves in terms of uncertainties on Stokes parameters, resulting in systematic effects on DOP and AOP. While the POLDER team has evaluated the measurement uncertainty in parameter U in the principal plane,[9] to the best of our knowledge no direct evaluation of the systematic errors in the DOP and AOP has been performed, which motivated this

work. In Sections 2.1 and 2.2 we will adopt two, in a sense, opposite approaches to determining the noise on DOP and AOP. In determining systematic errors on DOP will will try to minimize, as much as possible, the external scattering events in order to isolate the lowest DOP values possible. This will establish the maximum limit on DOP noise, as the lower the DOP values are the higher is the DOP uncertainty (see, e.g., Ref. 15, 16), with the obvious implication that higher DOP values have lower DOP uncertainty. On the other hand, in determining the systematic errors on AOP we will make use one of the most highly polarized Earth viewing scenes possible, the clear-sky ocean in the forward scattering region. As the AOP will be shown to be relatively stable across the entire dynamic range of the POLDER measurements, a sharply peaked AOP would allow us to more precisely determine the bias. As the single scattering assumption describes this type of scene well, a systematic deviation of ψ from 90° is a sign of bias in AOP. In Section 3 we use the DOP and AOP biases calculated in the previous sections to evaluate their impact on the calculated reflectance ρ_0. While our study is applicable to the entire polarization domain, we will refer to the CPF-VIIRS $\mathrm{DOP} < 0.1$ regime wherever relevant.

2 Determining the DOP Systematic Effects in DOP and AOP

In this study we consider two types of atmospheric conditions: overcast and clear. We will rely on the former to estimate the bias in the degree of polarization, while the latter will be used to evaluate the bias in the determination of the angle of polarization. In both cases we pick the extremes: in order to determine the bias in DOP we will require as unpolarized sample as possible, while to determine the bias in AOP we simply select the most polarized scene type characterized by the POLDER instrument. Unless otherwise indicated, the datasets shown throughout the text represent the entirety of 2006 POLDER data, subject to scene constraints, such as cloud or scene type, but without solar or view geometry restrictions.

2.1 Systematic Error in DOP

In order to better understand the influence of the noise on DOP, we illustrate it with the "toy" Monte Carlo simulation. Sets of three random values from three Gaussian distributions representing Q, U and I Stokes parameter measurements. The latter have somewhat realistic means (i.e, comparable to POLDER data), but arbitrary standard deviations chosen only to better illustrate the influence of the noise. From each set of random Q, U and I values, the corresponding DOP was calculated using Eq. 1. The results are shown in Fig. 1. The same Gaussian means of $\bar{Q} = 0.01$, $\bar{U} = 0$, $\bar{I} = 0.5$, were used to generate all three DOP distributions, while $\sigma_Q = 0.02$, $\sigma_U = 0.03$ and $\sigma_I = 0.2$ were used to generate the top left plot, for top right plot σ_Q and σ_U were increased by a factor of two (σ_I was kept at the same value of 0.2), while for the bottom plot σ_I was increased by a factor of two, while keeping $\sigma_Q = 0.02$ and $\sigma_U = 0.03$, as in the top left plot. The comparison of the plots shows that convolving Q and U with additional noise, leads to a wider DOP distribution with a higher mean, while adding noise to radiance I has the effect of lowering mean DOP, but, since DOP values are always positive, the overall effect of noise is to always bias DOP towards higher values.

Turning towards the empirically observable polarization, its typical manifestations in the Earth's atmosphere are Rayleigh and Mie scattering, including rainbows, cloudbows and glories. For clear or partly cloudy conditions surface reflection and refraction are also significant contributors to polarized light. We would like to identify the as unpolarized sample as possible, with the assumption

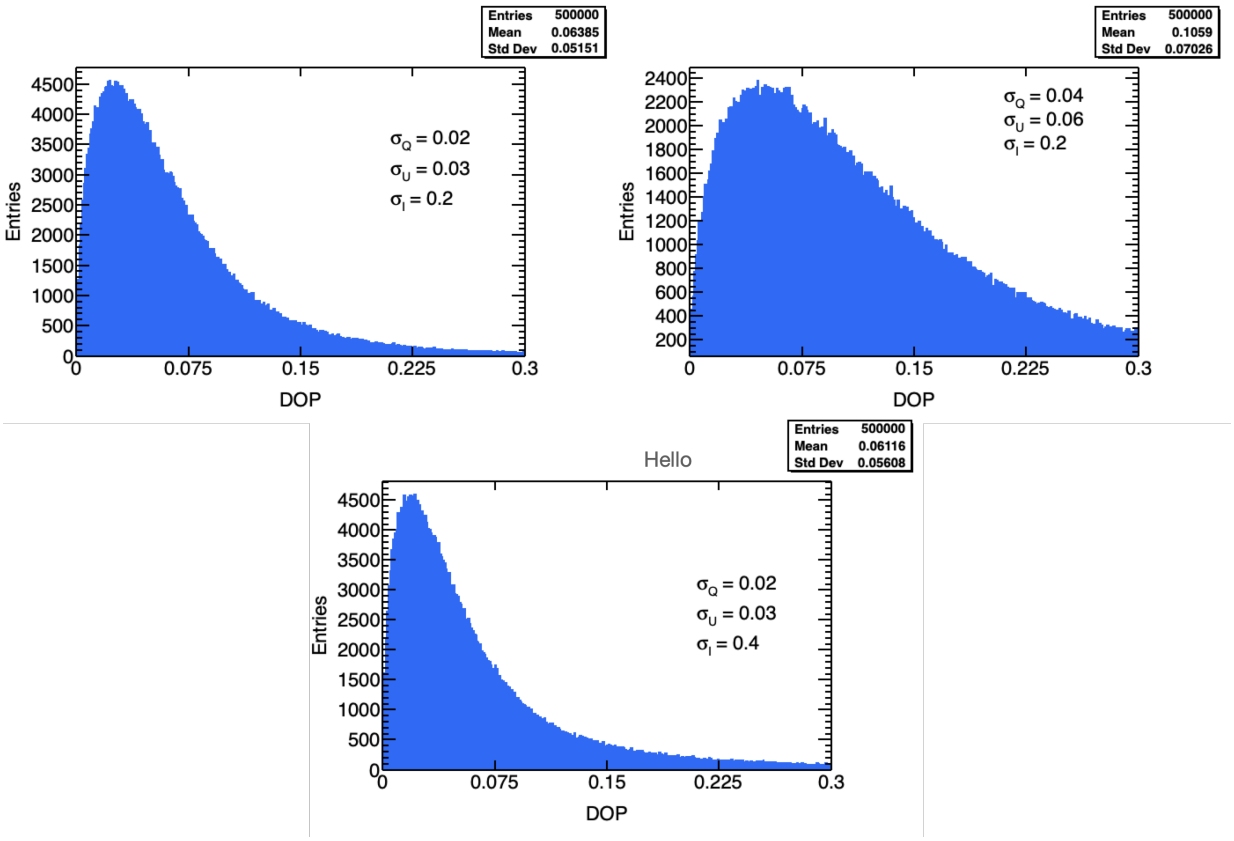


Fig 1 Illustration of the influence of noise on the Stokes parameters on DOP. The DOP distributions are computed from the "toy" Monte Carlo-simulated, Gaussian-distributed, normalized Stokes parameters Q, U and I. To generate all three DOP distributions same mean $Q = 0$, $U = 0$ and $I = 0.5$ was used, while the standard deviations were $\sigma_Q = 0.02$, $\sigma_U = 0.03$ and $\sigma_I = 0.2$ for the top left plot, $\sigma_Q = 0.04$, $\sigma_U = 0.06$ and $\sigma_I = 0.2$ for the top right plot, $\sigma_Q = 0.02$, $\sigma_U = 0.03$ and $\sigma_I = 0.4$ for the bottom plot.

that the remaining polarization is as close to the combination of photon and detector noise as the measured data allows. This is a conservative approach, since once we are reasonably sure that we have identified the lowest polarized dataset, the systematic uncertainty associated with higher levels of DOP will only be lower.[15,16] Among the observable candidate scene types we identify snow and ice surfaces, ice clouds and certain types of water clouds (see, e.g., Ref. 9). In terms of polarization characteristics, snow and ice surfaces are similar to ice clouds, but since our goal is to minimize scattering in the atmosphere and due to their relatively low sampling frequency, we disregard the ice- and snow-covered land surfaces. Of the remaining candidate datasets, in Fig. 2 we compare the DOP as a function of the cloud optical thickness (COT) of ice (left figure) and water (right figure) clouds over land for the 865 nm POLDER band. Our studies[17] indicate that for longer wavelengths, such as this one, DOP becomes less sensitive to the chosen land surface type, so a combination of vegetated and non-vegetated surface types is used here. From Fig. 2 two things become apparent: first, the contribution of the surface polarization is overcome by the increased scalar radiance for $\mathrm{COT} > 15$, where the mean and the standard deviations become nearly invariant. Secondly, while at some scattering angles ice clouds may be highly polarized, the average DOP is lower for ice clouds than for water clouds. Therefore, as we seek to minimize polarization in the samples used in this analysis, we discard the water cloud dataset and select only

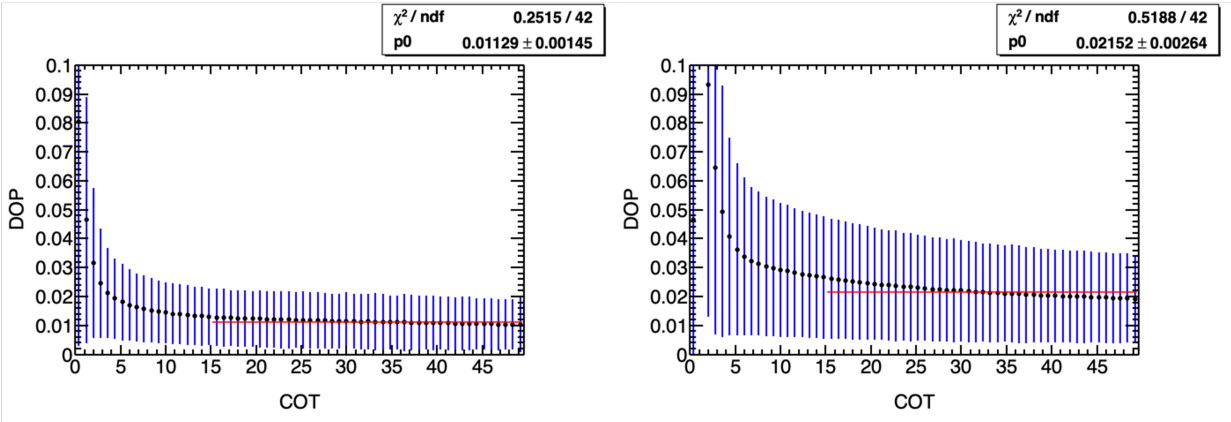


Fig 2 DOP *vs.* COT comparison between ice clouds (left) and water clouds (right) over land surfaces for the entirety of POLDER 2006 data. For clarity DOP bin averages and the corresponding standard deviations are shown in place of scatter plots. p_0 represents the fit parameter for zero-slope fit (solid red line) to the plot for $\mathrm{COT} > 15$.

the ice clouds for this analysis.

Comparing the zero-slope fits for the DOP *vs.* COT dependence for ice clouds over ocean in Fig. 3 with the left plot in Fig. 2, we note that at sufficiently large values of COT, $\mathrm{COT} > 15$, the atmospheric contribution dominates the surface contribution.

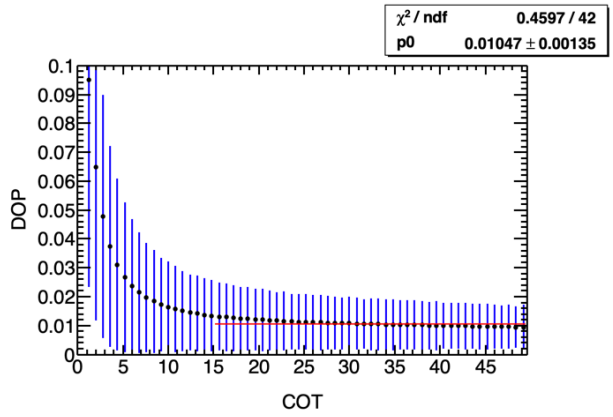


Fig 3 DOP *vs.* COT comparison for ice clouds over ocean. For clarity DOP bin averages and the corresponding standard deviations are shown in place of scatter plots. p_0 represents the fit parameter for zero-slope fit (solid red line) to the plot for $\mathrm{COT} > 15$. This plot is to be compared with ice clouds over land (Fig. 2, left).

Finally, to minimize the contribution of the atmospheric scattering we would like to verify whether the cloud top pressure influences our selection. In Fig. 4 we show how the data sample, which satisfied the previous constraints, is affected by cloud top height. For this selection we use the ice cloud top pressure measurements performed by the POLDER instrument itself.[18] After the initial plateau, one observes the increase in DOP for pressure higher than 300 hPa, likely due to increased atmospheric scattering lower in the atmosphere. To constrain DOP to the smallest values, the final selection contained data points corresponding to ice cloud top pressure of less than 300 hPa.

With the selection of the lowest polarized data sample finalized, we would like to find out at which view geometry the lowest polarization occurs. Parol, *et al.*[19] examined the behavior of

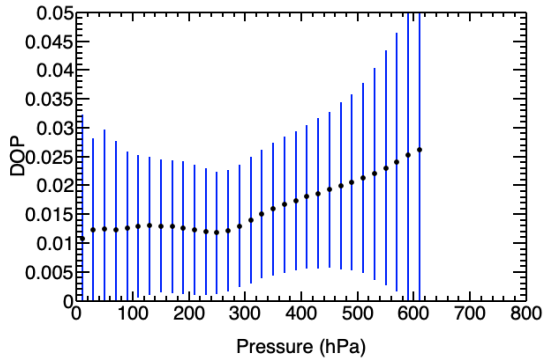


Fig 4 DOP *vs.* cloud top pressure dependence for ice cloud scenes. For clarity DOP bin averages and the corresponding standard deviations are shown in place of scatter plots.

polarized reflectance defined as

$$\rho_P = \frac{\pi\sqrt{Q^2+U^2}}{E_s}, \tag{7}$$

where E_s is the solar irradiance. Based on the simulated polarized reflectance for three different ice crystal shapes and the polarized reflectance measured during 1994 POLDER airborne campaign, the simulated reflectance crosses the point of zero-polarization (with the choice of axes corresponding to $U = 0$) at the scattering angle around $160°$ to $170°$, known as "neutral point", while the measured (unsigned) polarized reflectance shows a minimum around the same scattering angle of $170°$. This conclusion is consistent with our results plotted in Fig. 5 in terms of the DOP *vs.* scattering angle for the 865 nm channel.

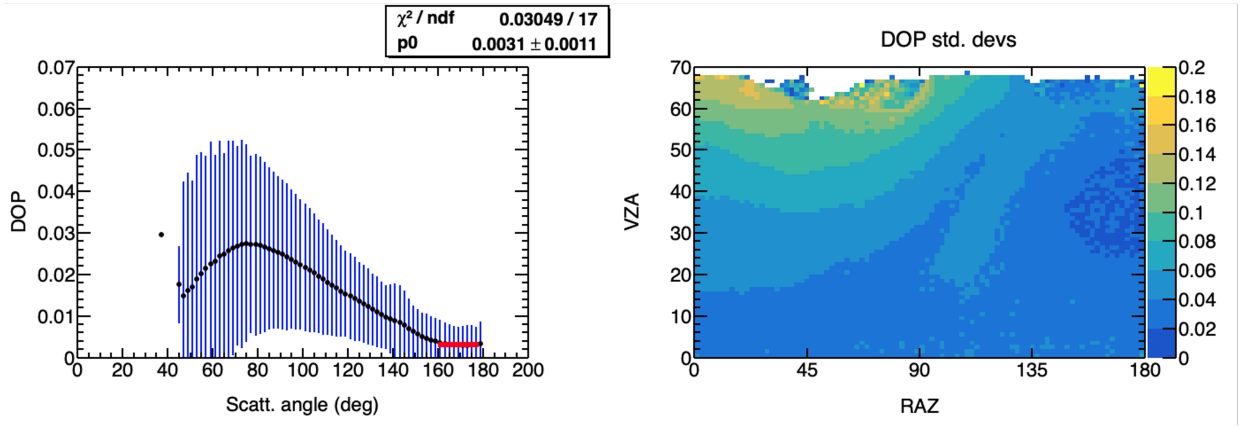


Fig 5 Left: DOP *vs.* scattering angle is plotted for the dataset identified by earlier filters (865 nm POLDER band). For clarity per-bin DOP means and standard deviations are shown in place of a scatter plot. The plateau for scattering angles greater than $160°$ is at the limit of POLDER resolution, as well as an indication of maximum determined bias $p_0 = 0.0031$ determined from the zero-slope fit (solid red line). Right: for comparison typical DOP standard deviations associated with the ePDM for $30° < \mathrm{SZA} < 40°$ for the same, 865 nm band, are shown. Standard deviations driven by natural variability clearly dominate over the systematic uncertainty shown on the left plot.

The fit around the neutral point in Fig. 5 (left) indicates that the DOP bias for the 865 nm is $\Delta_{P_{865}} = 0.003 \pm 0.001$, where the uncertainty is the error on the mean. The fact that in our least

polarized dataset the neutral point never exactly reaches $\rho_p = 0$ is an indication of the bias present in DOP determination. On the right-hand size of Fig. 5 a representative distribution of the standard deviations associated with an ePDM for 865 nm band and $30^\circ < \mathrm{SZA} < 40^\circ$ constraint is shown. Standard deviations of 0.02 and above seen to dominate, with the lowest standard deviations of the order of 0.01 occurring in the backscatter region around $150^\circ < \mathrm{VZA} < 180^\circ$. Comparing the left and the right Fig. 5 we observe an order of magnitude, or greater, difference between the typical standard deviations and the systematic error. The same observation holds true for other SZA ranges and rest of the polarized POLDER bands.

Repeating the procedure for the other two POLDER bands, for the 670 nm the DOP bias was found to be 0.008 ± 0.002, while for 490 nm the bias is 0.007 ± 0.001. We note that while these two results are consistent, the DOP bias for the 865 nm channel found earlier appears to be significantly lower than both of those values. While polarized radiance $I_p \equiv \sqrt{Q^2 + U^2}$ was determined to be consistent within 10% across all three channels, the 865 nm channel has a bandwidth of 34 nm, which is approximately twice that of the 490 and 670 nm.[9]

2.2 Systematic Error in AOP

As mentioned in the introduction, angle of polarization in the scattering plane ψ and the angle of polarization relative to the local (spacecraft) plane of reference AOP (χ) are related and may be expressed solely in terms of view geometry.

In order to determine the systematic error in the angle of polarization, we adopt the approach opposite, in a sense, to how the systematic error in DOP was determined by selecting the most highly polarized scene types available to us, the clear-sky ocean scene. The choice of the clear-sky ocean scene is motivated by the fact that due to the high polarization in the ocean's forward scatter region the mean ψ may be determined with higher accuracy due to the higher mean and lower standard deviation of its probability density distribution (essentially, higher signal-to-noise ratio) than for other scene types, such as, for example, overcast scenes. The fact that the mean, however, does not vary significantly across the dynamic range is evidenced by ψ vs. radiance plot in Fig. 6. Although the clear-sky ocean scene is used to plot Fig. 6, the other scene types show the same average biased mean across the radiance domain, albeit the accuracy of that mean is lower due to higher uncertainties. To ensure that the highest polarization is selected we constrain the wind speed to be between 2 and 10 m/s and for the 670 nm and 865 nm channels, where the aerosol optical depth was measured, we restrict the aerosol optical depth (AOD) to lie between 0 and 0.02. To enhance the single scatter signal we restrict the view geometry to the forward region, i.e., where the scattering angle $\Theta < 90^\circ$. With the assumption that the uncertainties in view geometry variables are negligible, from Eq. 3 the mean bias in AOP is approximately equal to the bias in ψ. Using the AOP obtained from POLDER data we may obtain ψ for all three POLDER bands. In Fig. 7 we show the ψ distribution for the 865 nm POLDER band.

From the left Fig. 7 the bias in ψ from the 865 nm POLDER band is 2.2°. For 490 nm this bias was found to be 0.5° and 2.0° for the 670 nm band. Since the angle of polarization χ, and, therefore, the variable ψ, is proportional to $\tan(U/Q)$, the deviation of ψ from 90° is due to the biased means of the Q and U Stokes distributions. This conclusion is confirmed by the relative independence of ψ on radiance (Fig. 6). Similarly, a "toy" Monte Carlo simulation, analogous to the the one in Fig. 1, shows that only varying the means, but not the widths, of U and Q distributions can alter the ψ mean. The biases are likewise unchanged if we limit the DOP to less

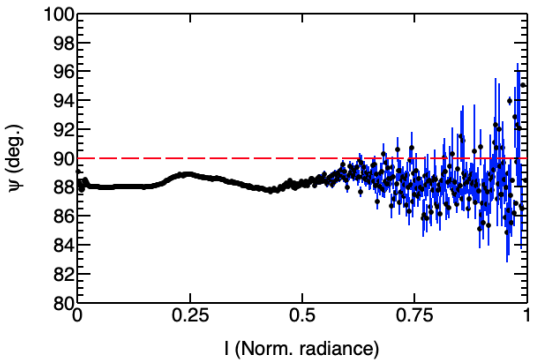


Fig 6 Angle ψ *vs.* normalized radiance shown for the the clear-sky ocean scene at 865 nm, where for clarity per-bin ψ means and error of the means (standard errors) are shown in place of a scatter plot. Clear bias away from $\psi = 90°$ is seen across the entire dynamic range.

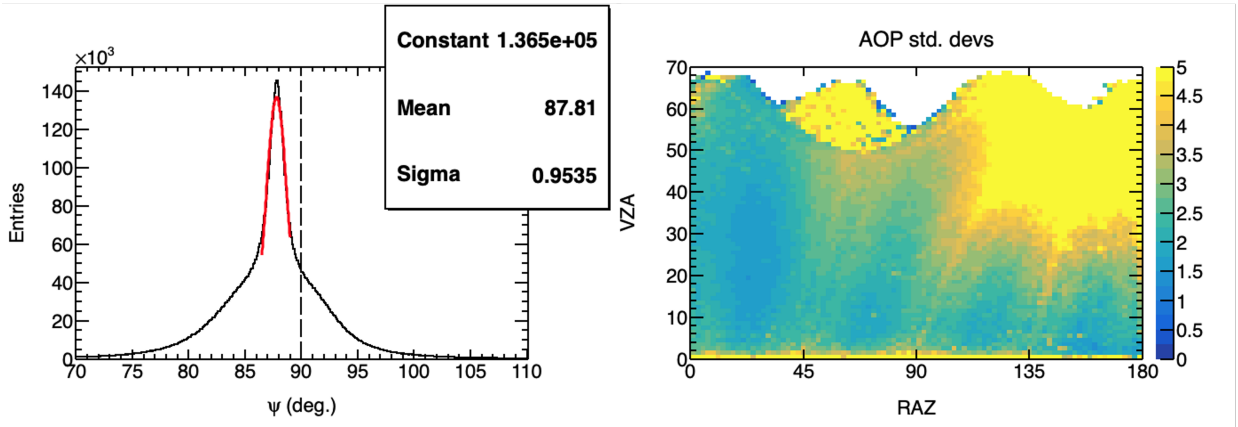


Fig 7 Left: Distribution of the ψ variable defined in Eq. 3 for the 865 nm POLDER band. The $2.2°$ shift obtained from the deviation of the mean of the Gaussian fit (solid red line) from $\psi = 90°$ is comparable to the AOP standard deviations for the 865 nm band ePDM ($50° < \text{SZA} < 60°$) shown on the plot on the right. Note that these plots are an AOP analogy to the DOP plots in Fig. 5.

than 0.1, as we will in the first year of CPF-VIIRS intercalibration. On the right-hand side of Fig. 7, we show the standard deviations for the ePDM corresponding to the 865 nm band with the $50^\circ < \mathrm{SZA} < 60^\circ$ constraint. Comparing the left-hand and right-hand figures reveals that, unlike for the DOP comparison in Fig. 5, the AOP uncertainties (especially in the forward region) are driven to a large extent by the systematic errors. In the next section we examine the effect the systematic errors have on the uncertainties in the VIIRS/CPF intercalibration. To summarize, the results shown in this section show that the angles of linear polarization derived from data are systematically lower than the "true" values of AOP for all three POLDER bands.

3 Effect of Systematic Uncertainties on Intercalibration

A combination of a polarized scene type ($P > 0$) and polarization-sensitive optics causes a bias in the measurement of the radiance or reflectance. This bias would cause the correction factor in Eq. 6 to deviate from unity. We would like to examine the effects of the systematic errors determined in the previous section have on c_ρ. While the realistic DOP depends on the scene type and view geometry, and the diattenuation coefficient on the detector band and optics configuration, we consider a somewhat artificial scenario where a and P are constant and independent of viewing conditions. We set DOP to $P = 0.1$, the threshold value for the first year of the CPF-VIIRS intercalibration, while a is set to 0.06, which is equal to the largest measured NOAA-20 VIIRS pre-launch parameter.[5] We take the realistic AOP distribution determined from POLDER data. Under such conditions, and assuming optical phase angle of 0, the correction factor, in terms RAZ and VZA, looks like the one shown in Fig. 8. The largest deviations from unity are $c_\rho = 1.006$ and 0.094. In principle, one can correct for the bias in the reflectance caused by DOP and AOP

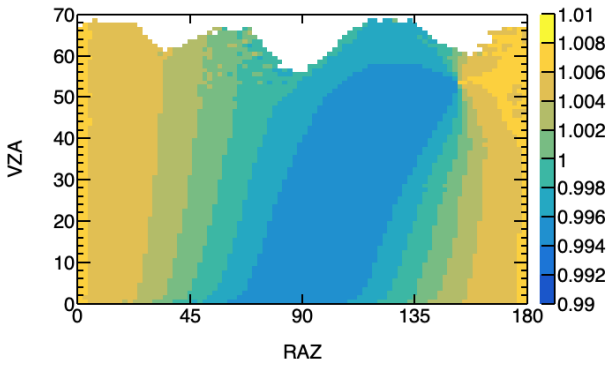


Fig 8 Reflectance correction factor c_ρ for the hypothetical "worst-case" scenario of $P = 1$ and χ calculated from POLDER data. The diattenuation coefficient a was set to 0.06. For this figure SZA was restricted to lie between 50° and 60°.

biases by shifting both by $P \to P - \Delta P$ and $\chi \to \chi + \Delta\chi$. Fig. 9 demonstrates the effect of such transformations on the reflectance correction factor c_ρ (Fig. 8) by plotting the residual differences before and after applying the $\Delta P = 0.008$ and $\Delta\chi = \Delta\psi = 2^\circ$ biases for the 670 nm band from Sections 2.1 and 2.2). The residual maxima and minima given for the 670 nm band found in Fig. 9 are $\pm 6 \times 10^{-4}$, and they are $\pm 4 \times 10^{-4}$ and $\pm 5 \times 10^{-4}$ for the 490 and 865 nm, respectively. We note that only the location in RAZ/VZA space, but not the magnitude, of the maxima and minima of the residuals vary with SZA, so that these maxima and minima are valid across the entire view

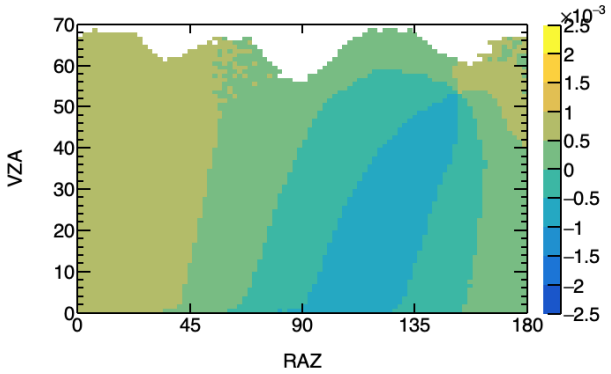


Fig 9 Residual differences between c_ρ (shown in Fig. 8) corrected for systematic bias in two polarization parameters, DOP and AOP, for the 670 nm band and uncorrected c_ρ.

geometry domain. Comparing these residual differences even with the previous results in Ref. 12 for low-polarized scenes, such as ice clouds, and an order of magnitude lower diattenution coefficient than used here, we find that for the CPF-VIIRS intercalibration samples with their $P < 0.1$ requirement, the influence of the systematic errors will be negligibly small.

Conclusions

The CPF intercalibration team has used POLDER measurements to construct a PDM database to estimate the polarization parameters for the CPF-VIIRS intercalibration samples. As absolutely unbiased measurements are not possible, it is imperative to evaluate the contribution of the systematic errors introduced by the POLDER instrument in the estimation of DOP and AOP, and their potential impact on the intercalibration uncertainty. In this work, we have quantified the expected systematic errors in the DOP and AOP using POLDER's three polarized channels. The systematic errors evaluated here are found to be less than 0.01 in DOP, which is roughly an order of magnitude smaller than the typical variability of most scene types, and is less than 2.2° in AOP, for all three channels. We also considered how the systematic errors in DOP and AOP may affect the at-sensor reflectance measurements under a somewhat artificial scenario of a completely polarized scene and a polarization-sensitive detector. While, given a highly polarization-sensitive detector channel, as well as certain geometries and highly polarized scene types, a correction due to DOP and AOP bias would make a difference, we found that for most VIIRS bands and our selection of intercalibration samples over low-polarized ($P < 0.1$) Earth scenes and geometry, the effect of these systematic errors on the CPF-VIIRS intercalibration will be negligible.

Disclosures

The authors are supported by CLARREO Pathfinder project funding from the NASA Earth Science Division in the Science Mission Directorate. The authors declare that they have no conflict of interest.

Acknowledgments

The authors would like to thank the anonymous reviewer and François-Marie Bréon of Laboratoire des Sciences du Climat et de l'Environnement (France) for their invaluable critique that has greatly

helped to improve this article. The authors also thank PARASOL data distribution centers at CNES and ICARE, France, for providing access to their data.

Data, Materials, and Code Availability

Data used in this work may be found on the POLDER/PARASOL Data and Services on the ICARE website hosted by the University of Lille (France).

References

1 Y. Shea et al., "Clarreo Pathfinder: Mission Overview and Current Status," *IGARSS 2020 - 2020 IEEE International Geoscience and Remote Sensing Symposium*, Waikoloa, HI, USA, 2020, pp. 3286-3289, doi: 10.1109/IGARSS39084.2020.9323176.

2 Wielicki, B.A.; Barkstrom, B.R.; Harrison, E F.; Lee, R.B.; Smith, G.L.; Cooper, J.E. "Clouds and Earth Radiant Energy System (CERES): An Earth Observing System Experiment." *Bull. Am. Meteorol. Soc.* **77**, 853–868, doi:10.1175/1520-0477(1996)077¡0853:CATERE¿2.0.CO;2, 1996.

3 Lee, T.E.; Miller, S.D.; Turk, F.J.; Schueler, C.; Julian, R.; Deyo, S.; Dills, P.; Wang, S. "The NPOESS VIIRS Day/Night Visible Sensor" *Bull. Am. Meteorol. Soc.* **87**, 191–200, doi:10.1175/BAMS-87-2-191, 2006.

4 Sun, J.; Xiong, X.; Waluschka, E.; Wang, M. "Suomi National Polar-Orbiting Partnership Visible Infrared Imaging Radiometer Suite polarization sensitivity analysis." *Appl. Opt.* **27**, 7645–7658 doi:10.1364/AO.55.007645, 2016.

5 J. Sun, M. Wang, L. Jiang, and X. Xiong, "NOAA-20 VIIRS polarization effect and its correction," *Appl. Opt.* **27**, 6655-6665, doi:10.1364/AO.58.006655, 2019.

6 Lukashin, C., Z. Jin, G. Kopp, D.G. MacDonnell, and K. Thome, "CLARREO reflected solar spectrometer: Restrictions for instrument sensitivity to polarization." IEEE Trans. Geosci. Remote Sens., **53**, no. 12, 6703-6709, doi:10.1109/TGRS.2015.2446197, 2015.

7 D. Goldin and C. Lukashin, "Empirical polarization distribution models for CLARREO-imager intercalibration," *Journal of Atmospheric and Oceanic Technology* **33**, 439 – 451, doi:10.1175/JTECH-D-15-0165.1, 2016.

8 Deschamps, P.-Y.; Breon, F.-M.; Leroy, M.; Podaire, A.; Bricaud, A.; Buriez, J.-C.; Seze, G. "The POLDER mission: instrument characteristics and scientific objectives" *IEEE Trans. Geosci. Remote. Sens.* **32**, 598–615, doi:10.1109/36.297978, 1994.

9 B. Fougnie, G. Bracco, B. Lafrance, C. Ruffel, O. Hagolle, and C. Tinel, "PARASOL in-flight calibration and performance," Appl. Opt. **46**, 5435-5451, doi:10.1364/AO.46.005435, 2007.

10 Bréon, F.-M. *PARASOL Level-1 Product Data Format and User Manual*; Ed. 1, Rev. 4, 2016. Available online: PARASOL/ICARE.

11 F. Nadal and F.-M. Breon, "Parameterization of surface polarized reflectance derived from POLDER spaceborne measurements," *IEEE Transactions on Geoscience and Remote Sensing* **37**, 1709–1718, doi:10.1109/36.763292, 1999.

12 Goldin, D.; Xiong, X.; Shea, Y.; Lukashin, C., "CLARREO Pathfinder/VIIRS Intercalibration: Quantifying the Polarization Effects on Reflectance and the Intercalibration Uncertainty." Remote Sens. 11, 1914, doi:10.3390/rs11161914, 2019.

13 Zhang, Ying, Hao Wang, Heshen Li, Junhua Sun, Huilan Liu, and Yingshuo Yin. 2022. "Optimization Model of Signal-to-Noise Ratio for a Typical Polarization Multispectral Imaging Remote Sensor" Sensors 22, no. 17: 6624 doi:10.3390/s22176624.

14 Kopp, G. and Smith, P. and Belting, C. and Castleman, Z. and Drake, G. and Espejo, J. and Heuerman, K. and Lanzi, J. and Stuchlik, D., "Radiometric flight results from the Hyper-Spectral Imager for Climate Science (HySICS)," Geoscientific Instrumentation, Methods and Data Systems,**6**, 169–191, doi:10.5194/gi-6-169-2017, 2017.

15 A B Tibbs et al 2018, "Noise creates polarization artefacts," Bioinspir. Biomim. **13** 015005 doi:10.1088/1748-3190/aa9e22.

16 Simmons, J. F. L. and Stewart, B. G.,"Point and interval estimation of the true unbiased degree of linear polarization in the presence of low signal-to-noise ratios", Astronomy and Astrophysics, **142**, 100-106.

17 D. Goldin,R. Bhatt, and Y.Shea, "Empirical polarization distribution models for use in CLARREO Pathfinder-VIIRS intercalibration," (manuscript in preparation).

18 P. Goloub, M. Herman, H. Chepfer, J. Riedi, G. Brogniez, P. Couvert, and G. Séze, "Cloud thermodynamical phase classification from the POLDER spaceborne instrument," *Journal of Geophysical Research: Atmospheres* **105**, 14747–14759 doi:10.1029/1999JD901183, 2000.

19 F. Parol *et al.* , "First results of the POLDER Earth Radiation Budget and Clouds operational algorithm," in IEEE Transactions on Geoscience and Remote Sensing, **37**, no. 3, pp. 1597-1612, doi:10.1109/36.763273, 1999.

Biographies

Daniel Goldin received his B.S. degree in physics from the University of California, Santa Cruz, in 1995, the M.S. degree in physics from the University of California, Davis, in 1997, and Ph.D. in particle physics in 2005 from the University of Basel (Switzerland). He joined NASA on a contract as research scientist in 2013. His current research interests are in developing empirical Polarization Distribution Models (ePDMs) and their implementation into the CLARREO Pathfinder science framework.

Rajendra Bhatt received the M.S. degree and Ph.D. in electrical engineering from South Dakota State University and University of Virginia, respectively. He is currently supporting the CLARREO Pathfinder (CPF) project at NASA Langley Research Center as the Deputy Project Scientist for Intercalibration. Prior to joining the CPF team, he worked on the CERES project for 12 years developing techniques for in-flight calibration of geostationary and low earth-orbiting satellite imagers.

Yolanda Shea received her B.S. degree in Earth and Atmospheric Science from Cornell University in 2007 and her Ph.D. in Atmospheric and Oceanic Science from the University of Colorado at Boulder in 2012. She has been a research scientist at NASA Langley Research Center since 2012 with a focus on shortwave hyperspectral climate observations and is the Project Scientist for the Climate Absolute Radiance and Refractivity Observatory (CLARREO) Pathfinder (CPF) mission.